Supporting Information

Highly effective catalytic reduction of nitrobenzene compounds with gold nanoparticles-immobilized hydroxyapatite nanowire-sintered porous ceramic beads

Jie Li,[a] Minjie Wu,[a] Hongchen Du,[b] Buchuan Wang,[a] Yinglong Li,[a] and Weiwei Huan*[a]

[a] Zhejiang Provincial Key Laboratory of Chemical Utilization of Forestry Biomass, Zhejiang A&F University, Lin'an 311300, China.

[b] Shandong Peninsula Engineering Research Center of Comprehensive Brine Utilization, Weifang University of Science and Technology, Weifang 262700, China.

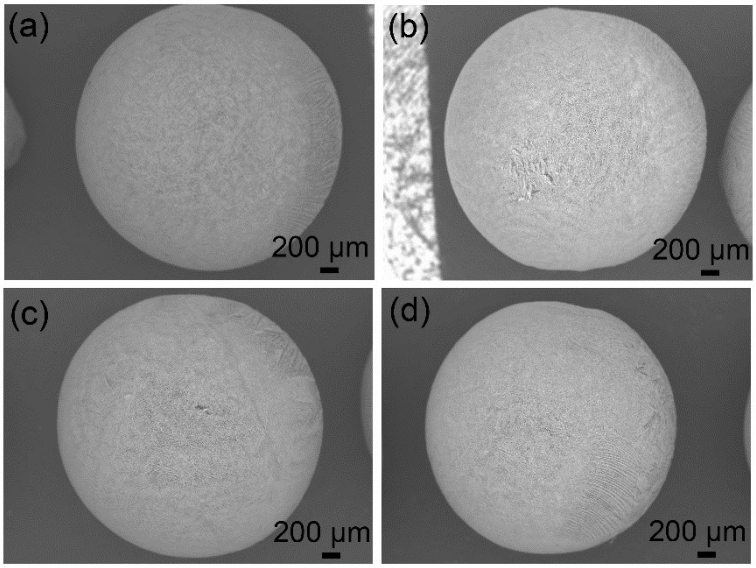

Fig. S1 (a−d) SEM images of HN/CS spheres.

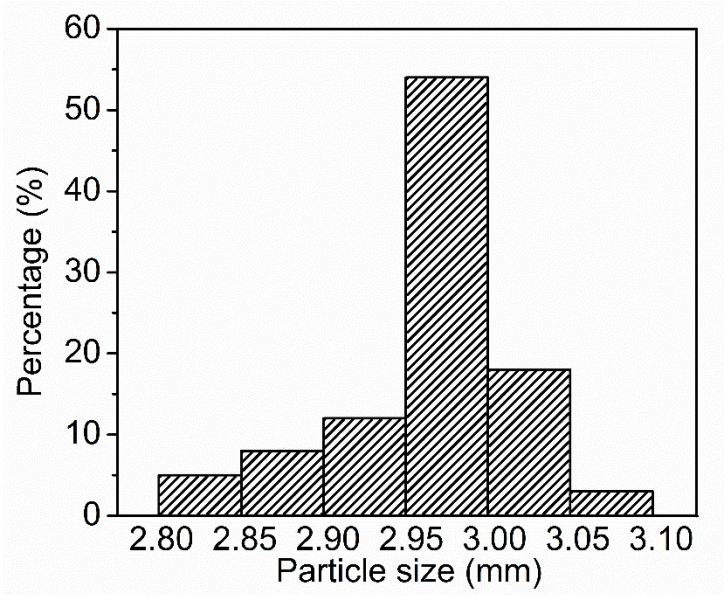

Fig. S2 The particle size distribution of HN/CS spheres. The average diameter of HN/CS spheres is calculated to 2.98 mm according to SEM images (100 particles).

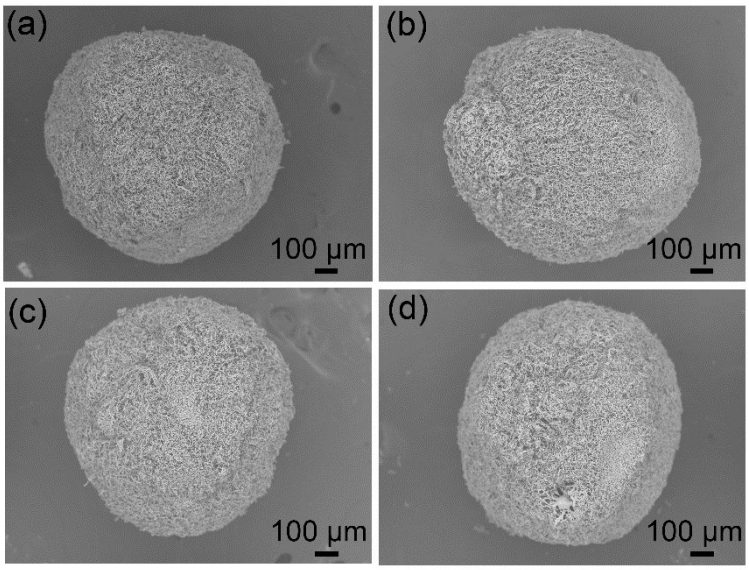

Fig. S3 (a−d) SEM images of HN porous ceramic beads.

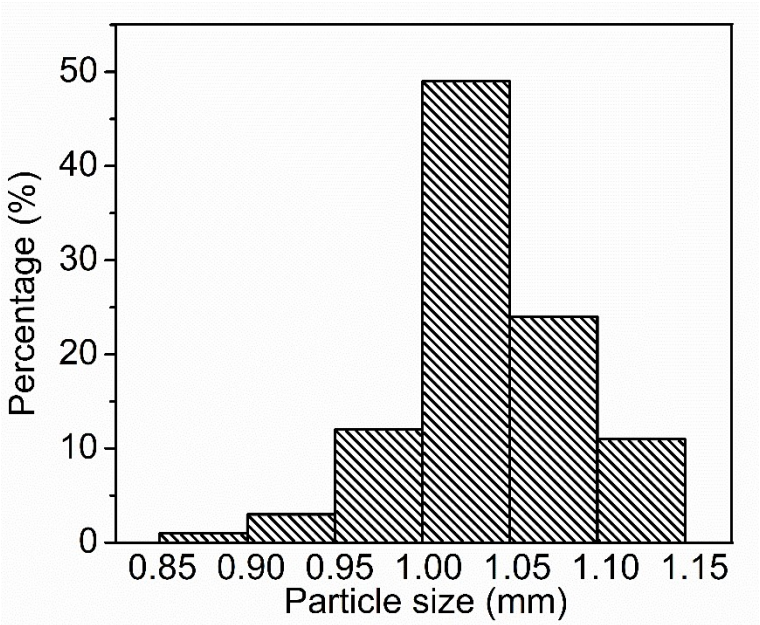

Fig. S4 The particle size distribution of HN porous ceramic beads. The average diameter of HN porous ceramic beads is calculated to 1.03 mm according to SEM images (100 particles).

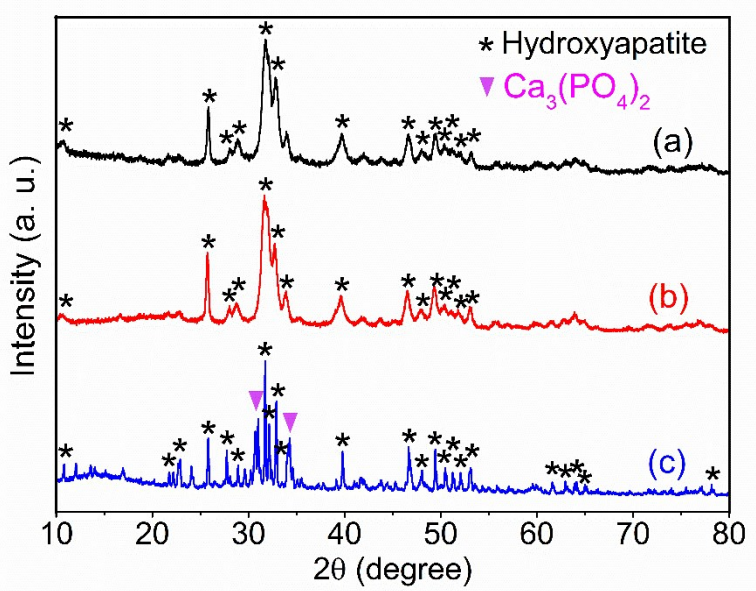

Fig. S5 XRD patterns: (a) HN, (b) HN/CS spheres, and (c) HN porous ceramic beads.

The diffraction peaks of HN can be indexed to the single crystal phase of hydroxyapatite (JCPDS no. 09-0432). The broadening of diffraction peaks can be explicated by the nanometer-sized diameters of HN. After hybridization with CS, the diffraction peaks of HN/CS spheres have hardly changed. Moreover, the XRD pattern of HN porous ceramic beads after sintering process has significantly changed. On the one hand, the widths of diffraction peaks become narrower than these of HN/CS spheres, showing the increased crystallinity and diameters of HN after sintering process. On the other hand, two additional characteristic diffraction peaks are observed, which can be assigned to the $Ca_3(PO_4)_2$ crystal phase, indicating that the partial phase transformation from hydroxyapatite to $Ca_3(PO_4)_2$ happens during the sintering procedure.

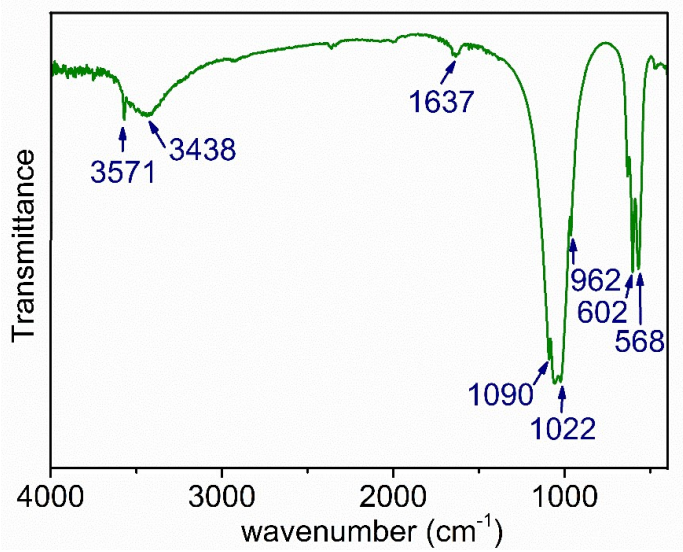

Fig. S6 FTIR spectrum of HN porous ceramic beads.

The characteristic absorption peaks at 1090, 1022, 962, 602, and 568 cm^{-1} correspond to the PO_4^{3-} group. The absorption peak at 3571 cm^{-1} is assigned to hydroxyl group. Additionally, an absorption peak at 1637 cm^{-1} and a broad absorption peak at 3438 cm^{-1} are ascribed to the adsorbed water.

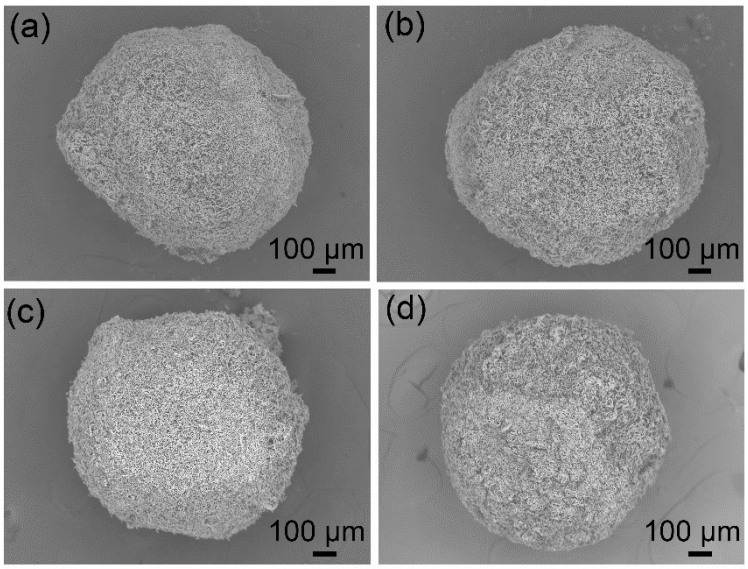

Fig. S7 (a−d) SEM images of HN/AuNP beads.

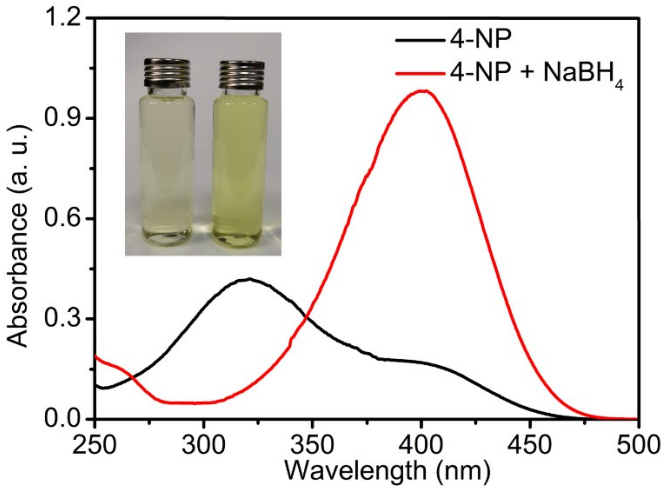

Fig. S8 UV-vis absorption spectra and digital images of aqueous solutions of 4-NP (left), and 4-NP and $NaBH_4$ (right).

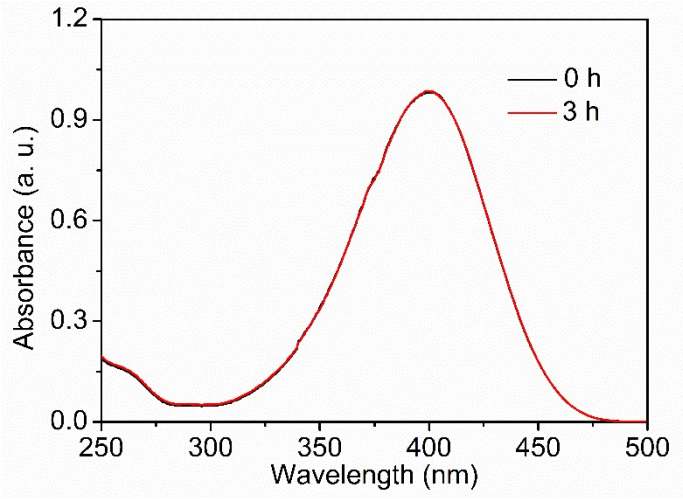

Fig. S9 UV-vis absorption spectra of aqueous solutions containing 4-NP and $NaBH_4$ for 0 h and 3 h.

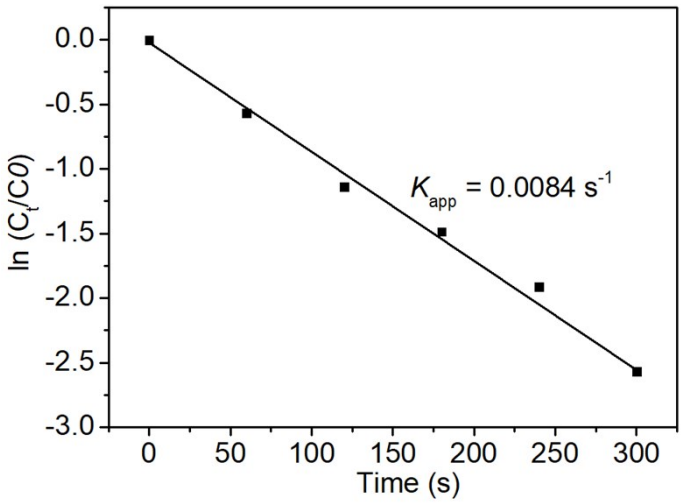

Fig. S10 Plots of C_t/C_0 *vs* the reaction time for the catalytic reduction of 4-NP to 4-AP using HN/AuNP (HN/AuNP-30) beads.

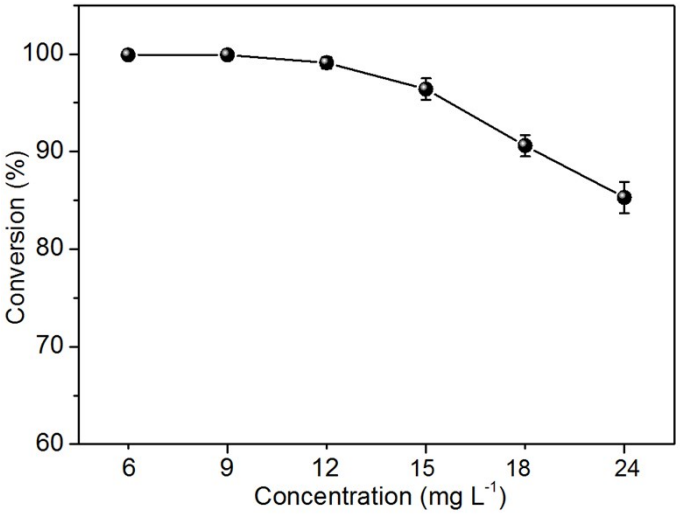

Fig. S11 The effect of initial concentration on the conversion efficiency of 4-NP to 4-AP.

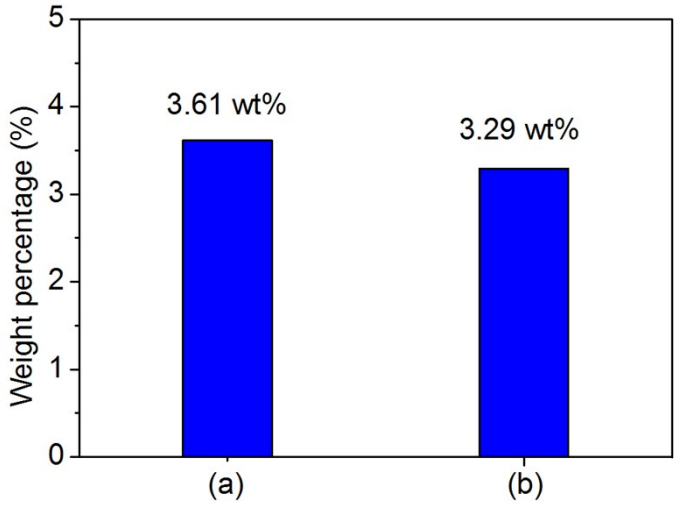

Fig. S12 ICP analysis results of AuNPs weight percentage of HN/AuNP beads before (a) and after (b) the continuous catalytic reaction for 15 cycles.

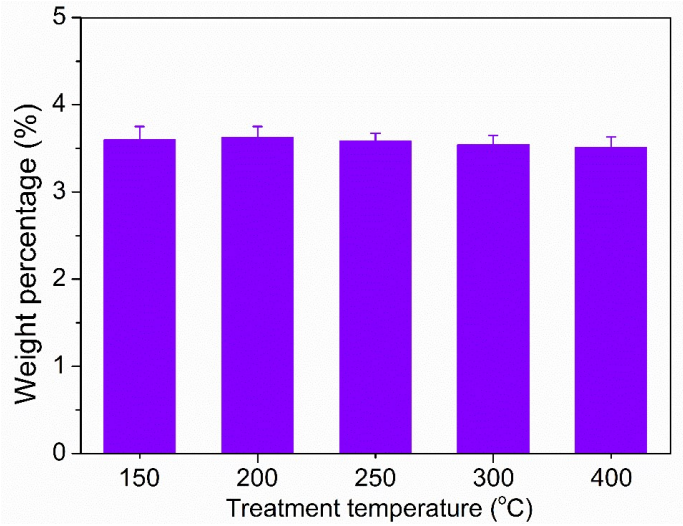

Fig. S13 ICP analysis results of HN/AuNP beads after heat treatment at different temperature for 1 h.

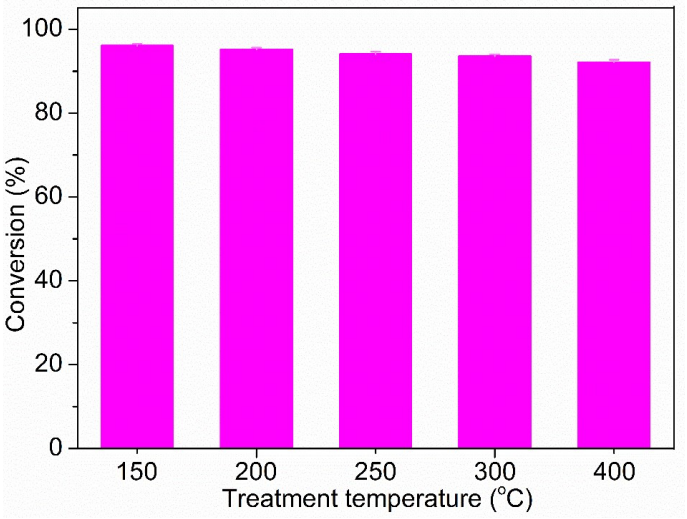

Fig. S14 Reusability of thermally treated HN/AuNP beads in recycling 15 times for catalytic degradation of 4-NP.

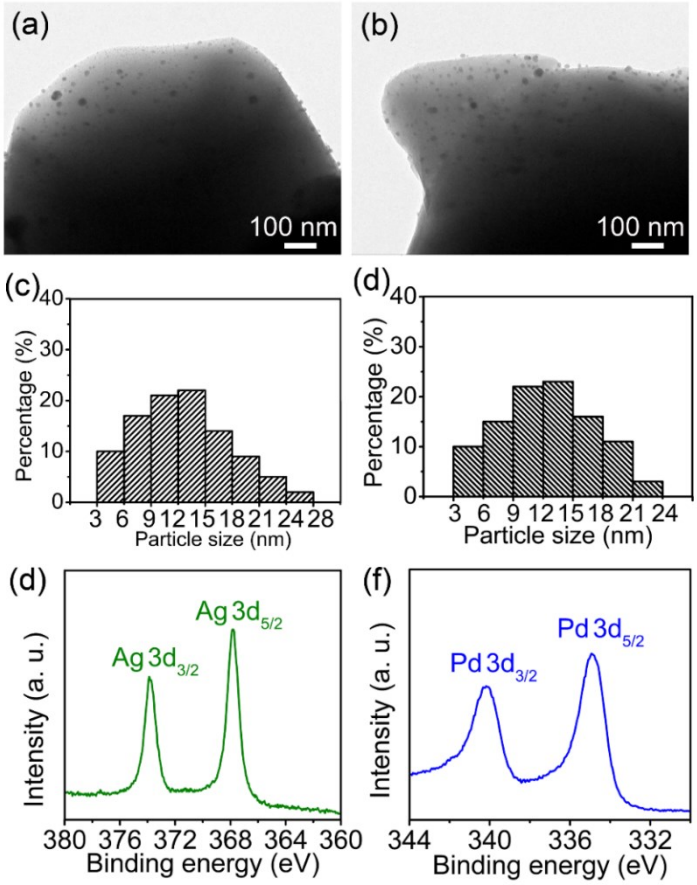

Fig. S15 Characterization results of HN/AgNP and HN/PdNP beads: TEM images of HN/AgNP beads (a) and HN/PdNP beads(b); (c) the particle-size distribution of AgNPs on HN/AgNP beads; (d) the particle-size distribution of PdNPs on HN/PdNP beads; XPS spectra: (e) HN/AgNP beads, and (f) HN/PdNP beads.

Table S1. Comparison of various catalysts for the reductive degradation of 4-NP.

Catalyst[a]	Support[a]	K_{app} (S^{-1})	Ref.
Au-PAAS	PAAS hydrogel	8.58×10^{-4}	16
Pd/γ-Fe_2O_3/p-Si	γ-Fe_2O_3/p-Si	2.65×10^{-3}	20
Au@C-loutus leaf	C-lotus leaf	9.33×10^{-3}	37
Pd@CHI	CHI	2.33×10^{-3}	38
Pd/PNGO30	PNGO30	2.83×10^{-3}	39
Pd/g-C_3N_4	g-C_3N_4	12.7×10^{-3}	40
Au@PAF-94	PAF-94	2.2×10^{-2}	41
Au@PAF-93	PAF-93	2.68×10^{-3}	41
Au/COF	COF	7.66×10^{-3}	42
Pd@h-mSiO_2	h-mSiO_2	6.0×10^{-3}	43
Fe_3O_4@nSiO_2@mSiO_2-Au	Fe_3O_4@nSiO_2@mSiO_2 nanochain	5.0×10^{-3}	44
SBA-15/PDA0.6/Ag	SBA-15/PDA0.6	7.34×10^{-3}	45
Au-PNIPAam hydrogel	PNIPAam hydrogel	4.83×10^{-3}	46

[a] PAAS = Sodium poly(acrylate); CHI = Cellulosic hydrogel anchoring 1,1,3,3-tetramethyl guanidinium-based ionic liquids moiety; PNGO = N-doped partially reduced graphene oxide; PAF = Porous aromatic frameworks; COF = Covalent organic frameworks; mSiO_2 = Hollow mesoporous silica nanotubes; PDA = Polydopamine; PNIPAam = Poly(N-isopropylacrylamide); p-Si = Porous Si.